**Supporting Information**

**Ms. ID: ACIE201302577**

**20 May, 2013**

21 pages

## Table of Contents



## Experimental

**Chemicals.** 98% Tris (2,2'-bipyridyl) ruthenium (II) chloride hexahydrate ($[Ru(bpy)_3]^{2+}$, Strem Chemicals, Newburyport, MA), was used as a fluorescent tracer in the desalination experiments. Poly(dimethylsiloxane) (PDMS) channels were prepared using a silicone elastomer and curing agent (Sylgard 184) from K.R. Anderson, Inc. (Morgan Hill, CA). Natural seawater was collected from Port Aransas, Texas, USA. Solutions of $Na_2SO_4$ were prepared from 99% sodium sulfate (anhydrous, Acros Organics, Fair Lawn, NJ) by dissolution in deionized water (18 MΩ•cm, Milli-Q Gradient System, Millipore, Bedford, MA). Solutions of NaCl were prepared from 99.5% sodium chloride (SigmaUltra, Sigma-Aldrich, St. Louis, MO) by dissolution in deionized water.

**Device fabrication.** The procedure for assembling the PDMS/quartz microfluidic devices is as follows. Pyrolyzed photoresist carbon (PPC)[1] microband electrodes were fabricated on quartz substrates (Technical Glass Products, Painesville Twp., OH) using AZ 1518 photoresist (AZ Electronic Materials, Somerville, NJ) and standard photolithographic techniques. The photoresist was spin coated onto the substrates at 500 rpm for 10 s, then 3500 rpm for 45 s, and finally 500 rpm for 5 s before being soft baked at 100 °C for 45 s. A mask aligner (Süss MicroTec, Garching, Germany) and photomask (CAD/Art Services, Inc., Brandon, OR) were used to achieve a desired electrode pattern on the substrate. The exposure was 10 s using a UV lamp intensity of 9.7 $mW/cm^2$. The substrates were then developed for approximately 12 s using AZ 400 K developer (AZ Electronic Materials) diluted 1/4 (v/v) with deionized water. The patterned photoresist substrates were then pyrolyzed in a quartz tube furnace (model 55035, Lindberg, Watertown, WI) with a forming gas of 5% $H_2$ and 95% $N_2$ (Regen, Praxair, Danbury, CT) continuously flowing at 100 sccm. The temperature was ramped from 25 °C to 1000 °C at a rate of 5 °C $min^{-1}$ and then held at 1000 °C for 1 h before cooling back to 25 °C. As previously described by our group, the PPC microbands undergo a decrease in width and thickness after pyrolysis.[2] A top-down optical microscope (Nikon AZ 100, Nikon, Tokyo, Japan) equipped with a CCD camera

(QuantEM:512SC, Photometrics, Tucson, AZ) was employed to determine the lateral dimensions of the PPC microbands. For conductivity and electric field measurements, PPC microbands were bonded to copper wires *via* larger bonding pads using conductive silver paste (62% weight solids, Electron Microscopy Sciences, Hatfield, PA) and then insulated with epoxy resin (5 minute epoxy, Devcon, Danvers, MA).

PDMS microchannels (desalination channel inlet 2.5 mm long, 100 $\mu$m wide, and 22 $\mu$m tall, desalination channel outlets 2.5 mm long, 50 $\mu$m wide, and 22 $\mu$m tall, auxiliary channel 5.0 mm long, 100 $\mu$m wide, and 22 $\mu$m tall) were fabricated from a single SU-8 2025 (MicroChem, Newton, MA) mold patterned on a silicon wafer (University Wafer, South Boston, MA). The separation between the parallel channels was 6.0 mm (center-to-center). The brine outlet branched from the desalted stream at a 30° angle (Scheme 1a, main text). Reservoirs were made using a 3 mm diameter metal punch to remove PDMS at each microchannel extremity. An optical profilometer (NT9100, Veeco, Plainview, NY) was employed to determine the height of the SU-8 microchannel mold. The PDMS channels were rinsed with ethanol and dried under $N_2$ before both the PDMS and quartz surfaces were exposed to an air plasma (60 W, model PDC-32G, Harrick Scientific, Ossining, NY) for 15 s on the medium setting, and finally the two parts were bound together with the BPE aligned at the channel centers and upstream of the

branched microchannel (Scheme 1a, main text). The PDMS/quartz microfluidic device was then placed in an oven at 65 °C for 5 min to promote irreversible bonding.

**Desalination experiments.** Before each experiment, a solution of seawater spiked with 20.0 $\mu$M $[Ru(bpy)_3]^{2+}$ was used to fill the desalination channel. The auxiliary channel was filled with seawater. To prevent obstruction of the microfluidic channel, sand and debris present in the seawater sample were removed *via* sedimentation before use. No other pre-treatment was required. Using a hand-held conductivity meter (Con 6, Oakton, Vernon Hills, IL), the seawater conductivity was measured to be ~50 mS/cm, which is an accepted value for seawater.[3] Pressure driven flow (PDF) was initiated by creating a solution height differential in the reservoirs at the ends of the channel by adding or removing seawater. Initially, 35 $\mu$L was added to the inlet reservoir of the desalination channel while 10 $\mu$L was added to each of the outlet reservoirs. This fill created a PDF (~0.08 $\mu$L/min) from inlet to outlets. A power supply (PWS4721, Tektronix, Beaverton, OR) was used to apply a 3.0 V bias between the desalination and auxiliary channels necessary to generate the electric field gradient for desalination. To ensure decoupling of the AC and DC circuits during the *in-situ* conductivity measurements, a 3.2 V battery pack (2 AA batteries, Duracell, Bethel, CT) was used to drive the desalination process. The

driving electrodes dipped into each reservoir were Pt wires. The fluorescent tracer was observed using an inverted epifluoresence microscope (Eclipse TE 2000-U, Nikon) fitted with a CCD camera (Cascade 512B, Photometrics). Images were collected and analyzed with image processing software (V++ Precision Digital Imaging, Auckland, New Zealand). When desired, either electric field or conductivity measurements were collected as the desalination proceeded.

**Electric field profile measurements.** The axial electric field profile within the desalination channel (Scheme 1a, main text) was monitored using a scanning digital multimeter (SDMM, Model 2700, Keithley Instruments, Cleveland, OH) equipped with a multiplexer module (Model 7701, Keithley). The acquisition time for each voltage measurement was ~0.1 s, and the voltage between pairs of microbands recorded every 2.0 s. To collect the axial electric field profile along the centermost ~3.2 mm of the 5.0 mm long microchannel, twelve PPC microbands (67 $\mu$m wide) were spaced ~323 $\mu$m apart (center-to-center). As depicted in Figure S-1, these microbands surround either side of the 82 $\mu$m wide BPE.

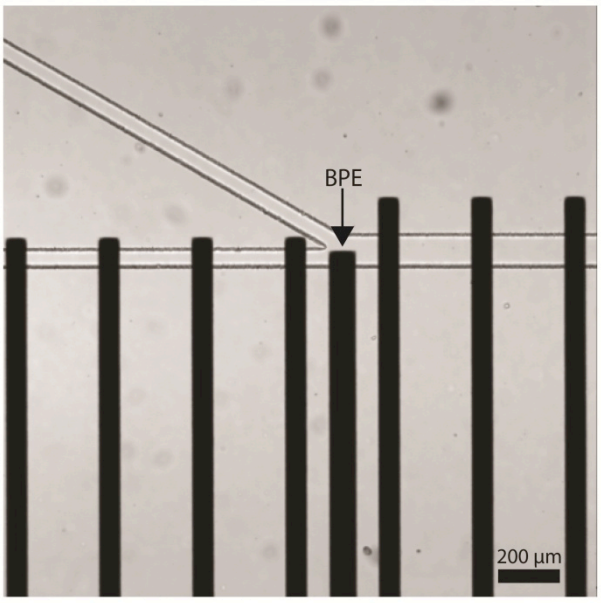


**Figure S-1.** Optical micrograph of PPC microbands and BPE device used to collect axial electric field measurements.

**Conductivity measurements.** *In-situ* conductivity measurements were performed using the bipolar pulse technique[4] with a method described by Soper and coworkers.[5] The solution conductivity in the desalted stream was monitored using a pair of PPC microbands (Figure S-2) and the circuit depicted below (Scheme S-1). All circuit components were assembled in-house. The exposed portion of the microbands were 50 $\mu$m long, 40 $\mu$m wide, and spaced by ~60 $\mu$m (center-to-center).

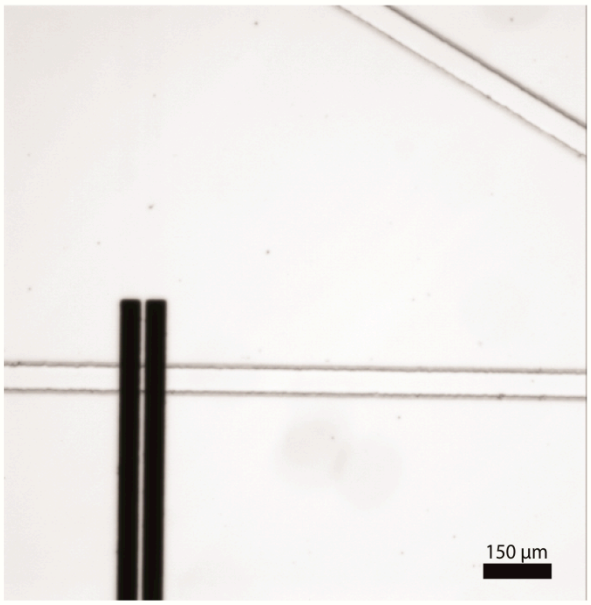


**Figure S-2.** Optical micrograph of PPC microbands embedded in the desalted stream used to collect *in-situ* conductivity measurements.

A function generator (Model 182A, Wavetek, San Diego, CA) was used to drive a ±0.75 V bipolar pulse at 5000 Hz through the upstream PPC microband, while the other microband was at virtual ground. As the signal is passed through the microchannel, the solution conductivity affects the current flow between PPC microbands ($V_o = -R_f i_f$), therefore modulating the output voltage ($V_o$) from the transimpedance amplifier with a feedback resistance ($R_f$) of 511, 400 Ω. Next, the signal is passed through a sample and hold amplifier. Using the trigger of the function generator (Wavetek) and a digital delay/pulse generator (Model DG535, Stanford Research Systems, Sunnyvale, CA), sample collection was

set to occur ~25 $\mu$s prior to the rising edge of the waveform. Data was collected for a total of 5 $\mu$s. The sampled signal was then passed through a second-order, 16 Hz low-pass filter before a multimeter (Model 2700, Keithley), operated with ExcelLINX software (Keithley), was used to collect the DC voltage measurement. The voltage was recorded every 0.5 s.

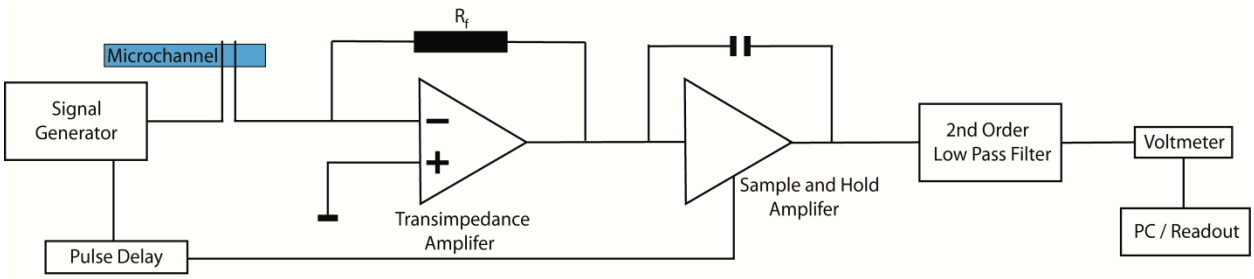


**Scheme S-1**

**Flow rate measurements.** PDF rates through the microchannel inlet and desalted stream (Scheme 1a, main text) were measured by monitoring the velocity of the fluorescent tracer after the power source was turned off. Total flow rates were approximately 0.08 $\mu$L/min from inlet to outlets. Flow through each of the branched streams was ~0.04 $\mu$L/min.

**Total current measurements.** The total current flowing through the device was monitored using the circuit depicted in Scheme S-2. As described previously, a power supply (PWS4721, Tektronix) was used to apply a 3.0 V potential difference between the desalination and auxiliary channels necessary to generate the electric field gradient for desalination. The driving electrodes

dipped into each reservoir were Pt wires. A multimeter (Model 6517B, Keithley) operated with a custom-written LabVIEW program (National Instruments, Austin, TX) was used to collect current measurements.

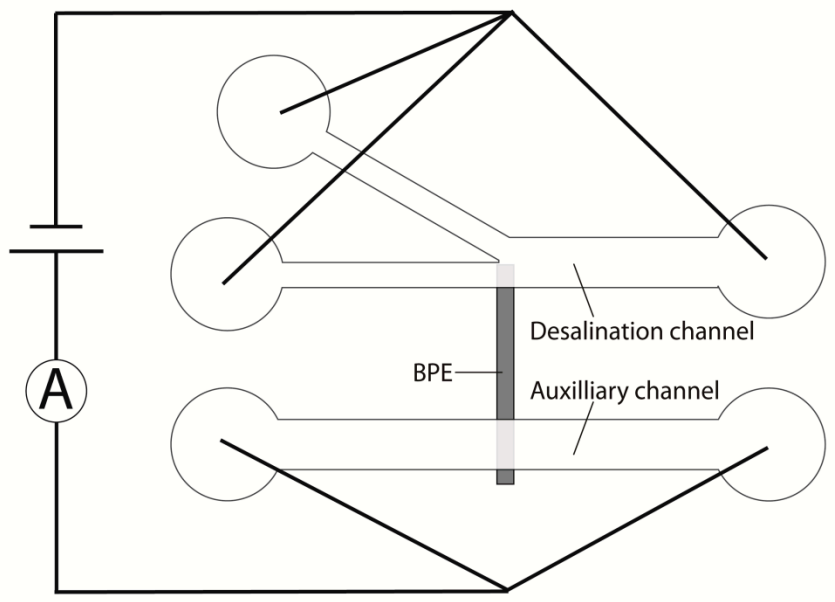


**Scheme S-2**

## Electric Field Strength Measurements

Axial electric field profile measurments were performed using the procedure described in the previous section. The SDMM data yields both positive and negative electric field measurements,[6] and therefore the data is presented as the absolute electric field strength for clarity. When the desalination channel is filled with seawater (red trace, Figure S-3) or 50 mS/cm NaCl (blue trace, Figure S-3), there is a sharp increase in the local

electric field strength near the BPE anode (centered at 2.5 mm) compared to when the channel is filled with 50 mS/cm $Na_2SO_4$ (black trace, Figure S-3). This measurement supports the notion that $Cl^-$ oxidation (eq 1, main text) is key to electrochemically-mediated desalination (EMD). Simulated axial electric field measurements (Figure 2b, main text) in 50 mS/cm NaCl reveal a peak field of ~14 kV/m, while the experimental measurement shown in Figure S-3 is lower: ~1.0 kV/m. However, when the simulated electric field strength is averaged over the same distance (323 $\mu$m) used in the experimental measurement, the simulated value, ~2.5 kV/m, is much closer to the measured value.

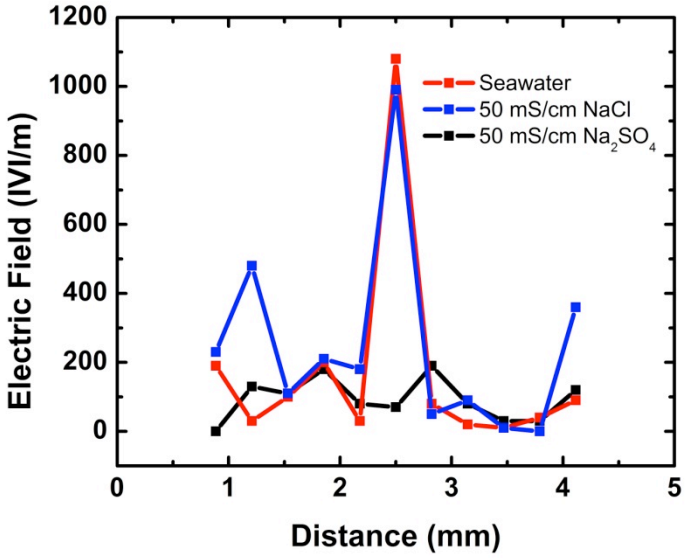


**Figure S-3.** Axial electric field measurements in the desalination channel with a 3.0 V bias between the desalination and auxiliary channels when filled with seawater (red trace), 50 mS/cm NaCl (blue trace), and 50 mS/cm $Na_2SO_4$ (black trace).

## Numerical Simulations

In this section we present the computational methods used to model the EMD of a 50 mS/cm NaCl solution. The three-dimensional geometry of the simulated system is exactly the same as that used for the experiments. The computer model simulated PDF initiated in the desalination channel as well as the distributions of local ion concentrations and local electric field. We assume $Cl^-$ oxidation is the faradaic reaction occurring at the BPE anode. The model was developed based on numerical schemes with inherent parallelism, allowing the straightforward implementation at modern high-performance computational platforms (supercomputers).

The model is based on equations describing the hydrodynamic, mass/charge transport, and electrostatic problems. Assuming that the liquid is incompressible, the local flow velocity field (**v**) can be described by the Navier-Stokes equation

$$\rho\left(\frac{\partial \mathbf{v}}{\partial t} + \mathbf{v}\cdot\nabla\mathbf{v}\right) = -\nabla p + \eta\nabla^2\mathbf{v}\,, \tag{S-1}$$

where $\rho$ and $\eta$ are the mass density and dynamic viscosity of the liquid, and p is hydrostatic pressure. Spatiotemporal variations in the concentrations of $Na^+$ and $Cl^-$ are governed by balance equations

$$\frac{\partial n_{Na}}{\partial t} = \nabla\cdot\left(D_{Na}\nabla n_{Na}\right) - \frac{F}{RT}\nabla\cdot\left(D_{Na}\nabla\phi\right) - n_{Na}\nabla\cdot\mathbf{v}\,, \tag{S-2}$$

$$\frac{\partial n_{Cl}}{\partial t} = \nabla \cdot \left(D_{Cl} \nabla n_{Cl}\right) + \frac{F}{RT} \nabla \cdot \left(D_{Cl} \nabla \phi\right) - n_{Cl} \nabla \cdot \mathbf{v} - r \,, \tag{S-3}$$

where n is the species concentration, D is the diffusion coefficient in the bulk fluid, $\phi$ is the local electric potential; F, R, and T represent the Faraday constant, molar gas constant, and temperature, respectively, **v** is the flow velocity, and r is the electrochemical reaction term describing a reduction in $Cl^-$ concentration due to faradaic reactions at the BPE anode.

The local concentrations of the species and the local electric potential are related by the Poisson equation

$$\nabla^2 \phi = -q_e \frac{n_{Na} - n_{Cl}}{\varepsilon_0 \varepsilon_r} \,, \tag{S-4}$$

where $q_e$ is the elementary charge, $\varepsilon_0$ and $\varepsilon_r$ are the vacuum permittivity and dielectric constant. We assumed that the hydrodynamic problem (eq S-1) can be decoupled from the species transport problem (eqs S-2 and S-3) and the electrostatic problem (eq S-4); i.e., that the density and viscosity of the fluid are independent of the ionic strength.

Instead of a direct numerical solution of eq S-1, the simulation of low-Reynolds number flow was performed with the lattice-Boltzmann method (LBM). In the LBM, a discretized version of the Boltzmann equation with linearized collision operator is solved.[7] The method simulates hydrodynamic phenomena by tracking the time evolution of distribution functions of fictitious particles that are confined to a spatial lattice and move with

discrete velocity, $\mathbf{c}_i$, during discrete time steps. The particle distribution function $f_i(\mathbf{r},t)$ represents the probability of finding a particle with velocity $\mathbf{c}_i$ at position $\mathbf{r}$ and time t. Each time step is divided into separate streaming and collision steps. Velocities $\mathbf{c}_i$ are chosen such that in one streaming step a particle moves along a lattice link from one lattice node to its neighbor. Subsequently, particle distribution functions $f_i$ are redistributed according to the discrete collision operator. The local fluid density $\rho(\mathbf{r},t)$ and velocity $\mathbf{v}(\mathbf{r},t)$ are obtained from the first-order and second-order moments of the particle distribution functions:

(S-6) $$\rho(\mathbf{r},t) = \sum_i f_i(\mathbf{r},t), \text{ and}$$

(S-7) $$\mathbf{v}(\mathbf{r},t) = \frac{\sum_i \mathbf{c}_i f_i(\mathbf{r},t)}{\rho(\mathbf{r},t)}.$$

At the solid-liquid interface, the no-slip boundary condition was implemented by application of the halfway bounce-back rule.[8] Usually, the LBM models are designated as DxQy, where x is the lattice dimensionality and y refers to the number of lattice links from a given lattice node to its neighbors (including the node itself) located on a simple cubic lattice. In this work, we used the D3Q19 lattice, a lattice with 18 links at each lattice node, which can be obtained by projecting the four-dimensional face-centered hypercubic lattice onto three-dimensional space.[9] It should be noted that we used the same

D3Q19 lattice also for the numerical solution of the transport equations (eqs S-2 and S-3) and the Poisson equation (eq S-4).

Transport equations were resolved with a numerical approach proposed by Capuani et al.,[10] which is based on identifying the species fluxes between neighboring nodes of a spatial lattice. The symmetric formulation of the flux between neighboring nodes ensures strict local mass/charge conservation. In that approach, the fluxes are the fundamental dynamical objects that couple external fields to both charged species concentration and fluid flow velocity. To resolve eqs S-2 and S-3, the following boundary conditions were imposed: (i) fluxes normal to the channel walls are zero for both charged species ($Na^+$ and $Cl^-$); (ii) the flux of $Na^+$ normal to the anodic BPE surface was zero; and (iii) the flux of $Cl^-$, $j_{Cl}$, normal to the anodic BPE surface was determined from a given current density across this surface

$$j_{Cl} = \frac{I_{BPE}}{S_{BPE}} \frac{1}{q_e}, \qquad \text{(S-8)}$$

where $I_{BPE}$ is the current through the BPE and $S_{BPE}$ is the contact surface area of the BPE anode with the solution.

The Poisson equation (eq S-4) was resolved by an under-relaxation finite difference method adapted to the D3Q19 lattice. Specifically, the weight coefficients, $\omega$, to determine the updated local value of the electric potential by accounting for its values in neighboring lattice nodes are

(S-9) $$\omega = \frac{1}{6\left(1+\sqrt{2}\right)} \text{ and } \omega = \frac{1}{6\left(2+\sqrt{2}\right)}$$

for the nearest and the next-nearest nodes, respectively. An under-relaxation coefficient of 0.25 was used to ensure numerical stability during calculation of the electrical potential in the region close to the BPE.

In this study, we performed simulations assuming the following values for the physical parameters: $\rho$ = 1.023 × $10^3$ kg/$m^3$, $\eta$ = 0.966 mPa·s , T = 298.16 K, $D_{Cl}$ = 2.032 × $10^{-9}$ $m^2$/s, $D_{Na}$ = 1.334 × $10^{-9}$ $m^2$/s, $\varepsilon_r$ = 78. The current through the BPE was assumed as $I_{BPE}$ = 50 nA and the BPE surface area ($S_{BPE}$) in contact with the solution in the desalination channel as $S_{BPE}$ = 82 $\mu$m × 50 $\mu$m (BPE width x length). The potential of the BPE was assumed to be 0.9 V and determined from the difference between the externally applied voltage (3 V) and the sum of the standard potentials for chloride oxidation and water reduction (1.3 V and 0.8 V). The concentrations of $Cl^-$ and $Na^+$ in the inlet reservoir of the desalination channel were assumed as 3.3121 × $10^{26}$ ions/$m^3$, which corresponds to a molarity of 0.55 M.

## Oxidation of PPC Anode

During seawater desalination, the primary processes occurring at the anode are $Cl^-$ and water oxidation, eqs 1 and 3 (main text), respectively. However, oxidation of the PPC anode may also occur if the applied potential is sufficient to drive this process.[11] If oxidation of the BPE anode occurs, it reduces the surface area of the electrode, thus limiting the time desalination can proceed once the anode has been entirely oxidized. Figure S-4a shows a PPC BPE anode before desalination. After ~10 min of desalination with a 3.0 V bias (Figure S-4b), the anode surface area is diminished, which indicates oxidation of the BPE is occurring. After ~30 min, the BPE anode is almost entirely oxidized (Figure S-4c).

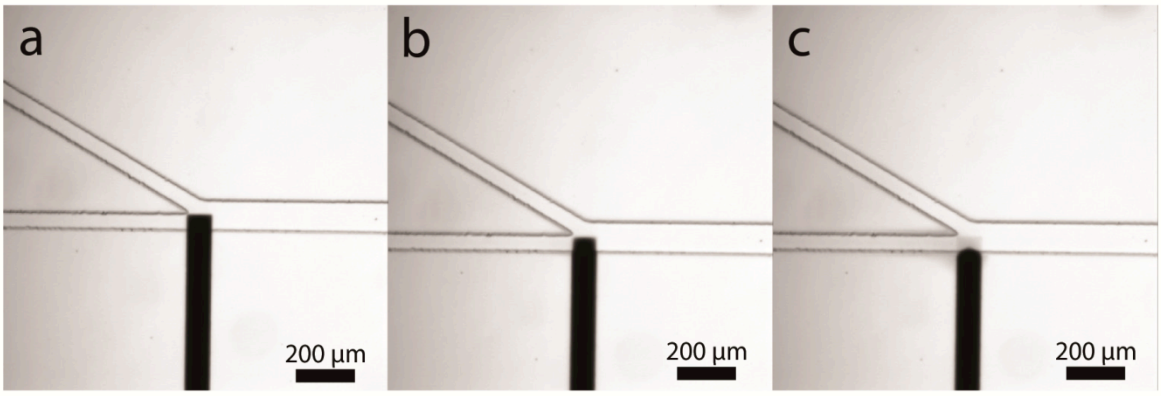


**Figure S-4.** Optical micrographs of a PPC BPE anode during a desalination experiment with a 3.0 V bias at 0 min (a), after ~10 min (b) and ~30 min (c).

Because of this instability, experiments reported here were limited to ~30 min. We are presently investigating the

feasibility of using alternative electrode materials that exhibit a higher degree of stability in seawater. Note too, that dissolution of the BPE may result in the formation of ions that lead to an increase in the local conductivity measured in the desalted stream. Therefore, the reported conductivities in the desalted stream and the extent of desalination should be viewed as minimums.

## ***In-Situ* Conductivity Measurements**

*In-situ* conductivity measurements were performed using the procedure described earlier. These measurements were correlated to the solution conductivity using a calibration curve of solution conductivity vs. the change in measured voltage ($\Delta E$). Figure S-5 shows a representative 4-point calibration curve ($R^2$ = 0.99) collected using seawater dilutions of known conductivity (previously measured with a hand-held conductivity meter, Oakton).

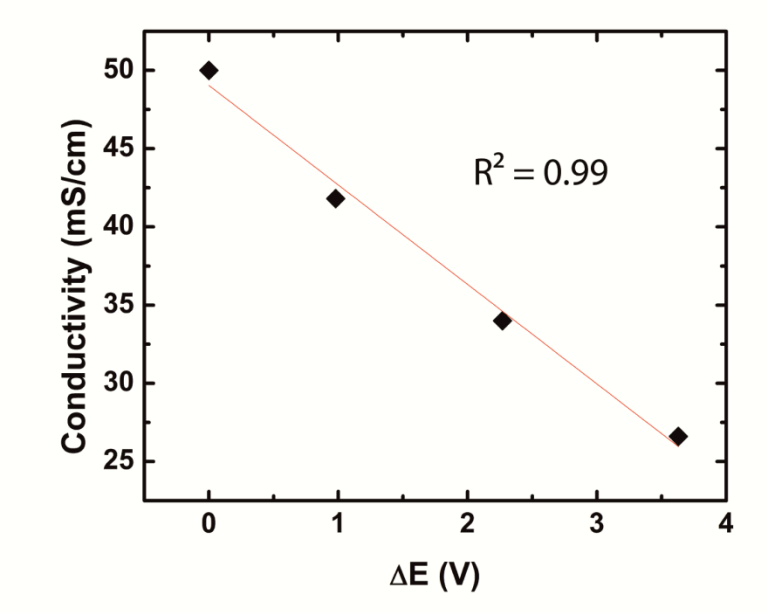


**Figure S-5.** A representative plot of solution conductivity vs. change in voltage (ΔE) for a desalination device.

To account for variations in device fabrication and response, each trial required a calibration curve to correlate changes in voltage to solution conductivity. The average conductivity in the desalted stream of five independently prepared devices was 37.5±2.5 mS/cm, indicating a ~25% salt rejection from the feed seawater. The conductivity of the feed seawater was 50 mS/cm.

## Percentage of Chloride Oxidized at BPE Anode

Assuming all current passing through the BPE anode goes toward $Cl^-$ oxidation, eqn S-10, where $i$ is current and $t$ is time, can be used to calculate the charge passed through the BPE anode ($Q_{passed}$).

(S-10) $Q_{passed} = it$

Using the plot of total current vs. time (Figure 3, main text), the steady-state current of the device is 20 nA. For a 50 s duration, the charge passing through the BPE anode can be calculated using eqn S-10, which yields $Q_{passed}$=1 x $10^{-6}$ C.

To calculate the total charge associated with $Cl^-$ present in the seawater ($Q_{present}$), eqn S-11 is employed, where $n$ is the number of electrons involved in the redox process, $F$ is Faraday's constant (96,485 C/mol), and $N$ is the number of moles of $Cl^-$.

(S-11) $Q_{present}=nFN$

Following eqn 1 (main text), $Cl^-$ oxidation is a 2 electron process, therefore $n$ = 2. The volume of seawater solution passing through the microchannel during a 50 s duration can be calculated by multiplying 50 s by the total volumetric flow rate through the device (~0.08 $\mu$L/min or 1.33 x $10^{-12}$ $m^3/s$). Knowing the concentration of $Cl^-$ in seawater (0.55 mol/L) then allows the number of moles of $Cl^-$ passing through the microchannel during a 50 s duration to be calculated ($N$ = 3.67 x $10^{-8}$ moles $Cl^-$). Using $n$, $F$, and $N$, the charge present from $Cl^-$ is found to be $Q_{present}$=7 x $10^{-3}$. Finally, dividing $Q_{passed}$ by $Q_{present}$ reveals that only ~0.01% of the total $Cl^-$ present in solution is oxidized at the BPE anode, assuming all current passing through the BPE anode goes toward $Cl^-$ oxidation.

## Energy Required for Pressure Driven Flow

To verify laminar flow in these microfluidic devices, the Reynolds number was solved using eq S-12, where ρ = density, V = linear flow velocity, h = channel height, w = channel width, and η = dynamic viscosity. With the constants[3] ρ = 1.023 g $cm^{-3}$ and η = 0.966 mPa·s for 35% seawater at 25 °C, the

(S-12) $$Re = \frac{\rho V \frac{2hw}{(h+w)}}{\eta}$$

$$Re = \frac{(1023\ kg\ m^{-3})(6.07 \times 10^{-4}\ m\ s^{-1})\ \frac{2\,(2.2 \times 10^{-5}\ m)(1.0 \times 10^{-4}\ m)}{(2.2 \times 10^{-5}\ m + 1.0 \times 10^{-4}\ m)}}{9.66 \times 10^{-4}\ kg\ m^{-1}\ s^{-1}} = 2.3 \times 10^{-2}$$

calculated Reynolds number is 2.3 x $10^{-2}$, indicating laminar flow through a rectangular channel.[12] Because seawater is nearly incompressible, the Poiseuille equation for pressure driven laminar flow in a rectangular channel (eq S-13)[13] can be used to solve for the pressure drop across the microchannel, where Q = volumetric flow rate, η = dynamic viscosity, L = channel length, h = channel height, and w = channel width. This equation assumes the ratio (h/w) approaches 0.

(S-13) $$\Delta P = \frac{12 Q \eta L}{h^3 w}\left(1 - 0.630\,\frac{h}{w}\right)^{-1}$$

$$\Delta P = \frac{12\,(1.33 \times 10^{-12}\ m^3\ s^{-1})\,(9.66 \times 10^{-4}\ kg\ m^{-1}\ s^{-1})\,(0.005\ m)}{(2.2 \times 10^{-5}\ m)^3\,(1.0 \times 10^{-4}\ m)}\left(1 - 0.630\,\frac{2.2 \times 10^{-5}\ m}{1.0 \times 10^{-4}\ m}\right)^{-1} = 84.4\ kg\ m^{-1}\ s^{-2}$$

Again, with $\rho$ = 1.023 g $cm^{-3}$ and $\eta$ = 0.966 mPa·s for 35% seawater at 25 °C,[3] $\Delta P$ = 84.4 kg $m^{-1}$ $s^{-2}$. The energy required to drive the PDF can be calculated by taking the pressure drop across the microchannel times the volumetric flow rate (eq S-14).

(S-14) $$\text{Energy for PDF} = (\Delta P \times Q)$$

$$\text{Energy for PDF} = (84.4\ \text{kg m}^{-1}\ \text{s}^{-2} \times 1.33 \times 10^{-12}\ \text{m}^3\ \text{s}^{-1}) = 1.12 \times 10^{-10}\ \text{W}$$

The power consumption required to drive the PDF necessary for desalination was determined to be 112 pW. In the main text, the power consumption necessary to drive EMD was found to be 60 nW, which yielded an energy efficiency of 25 mWh/L with a desalted flow rate of ~0.04 $\mu$L/min. However, to calculate the true efficiency of this device, the power associated with PDF must also be considered. This means the actual power consumption of this desalination technique is 60.11 nW, as opposed to 60 nW. Thus, the actual energy efficiency of the device is 25.05 mWh/L, as opposed to 25 mWh/L, indicating the energy required for PDF is minimal compared to that required to drive the electrochemical reactions necessary for desalination.

## References


[1] S. Ranganathan, R. McCreery, S. M. Majji, M. Madou, *J. Electrochem. Soc.* **2000**, *147*, 277-282.

[2] I. Dumitrescu, D. F. Yancey, R. M. Crooks, *Lab Chip* **2012**, *12*, 986-993.

[3] *CRC Handbook of Chemistry and Physics*, (Ed.: W. M. Haynes), 93 ed., CRC Press: USA, **2012**.

[4] D. E. Johnson, C. G. Enke, *Anal. Chem.* **1970**, *42*, 329-35.

[5] a) M. Galloway, W. Stryjewski, A. Henry, S. M. Ford, S. Llopis, R. L. McCarley, S. A. Soper, *Anal. Chem.* **2002**, *74*, 2407-2415; b) H. Shadpour, M. L. Hupert, D. Patterson, C. Liu, M. Galloway, W. Stryjewski, J. Goettert, S. A. Soper, *Anal. Chem.* **2007**, *79*, 870-878.

[6] a) J. M. Burke, C. F. Ivory, *Electrophoresis* **2008**, *29*, 1013-1025; b) K. N. Knust, E. Sheridan, R. K. Anand, R. M. Crooks, *Lab Chip* **2012**, *12*, 4107-4114.

[7] a) R. Benzi, S. Succi, M. Vergassola, *Phys. Rep.* **1992**, *222*, 145-197; b) S. Chen, G. D. Doolen, *Annu. Rev. Fluid Mech.* **1998**, *30*, 329-364; c) S. Succi, *The Lattice Boltzmann Equation for Fluid Dynamics and Beyond*. Oxford University Press: New York, NY, **2001**; d) *Lectures on Lattice Boltzmann Methods*, (Eds.: S. Ubertini, G. Bella, S. A. Orszag, S. Succi), Consorzio S.C.I.R.E.: Science4 Press, **2009**.

[8] M. A. Gallivan, D. R. Noble, J. G. Georgiadis, R. O. Buckius, *Int. J. Numer. Meth. Fluids* **1997**, *25*, 249-263.

[9] Y. H. Qian, D. d'Humières, P. Lallemand, *Europhys. Lett.* **1992**, *17*, 479-484.

[10] F. Capuani, I. Pagonabarraga, D. Frenkel, *J. Chem. Phys.* **2004**, *121*, 973-986.

[11] P. Takmakov, M. K. Zachek, R. B. Keithley, P. L. Walsh, C. Donley, G. S. McCarty, R. M. Wightman, *Anal. Chem.* **2010**, *82*, 2020-2028.

[12] A. E. Kamholz, P. Yager, *Biophys. J.* **2001**, *80*, 155-160.

[13] H. Bruus, *Theoretical Microfluidics*. Oxford University Press: USA, **2007**.